Journal of Solid State Chemistry 215 (2014) 8–15

Contents lists available at ScienceDirect

Journal of Solid State Chemistry

journal homepage: www.elsevier.com/locate/jssc

Calcination products of gibbsite studied by X-ray diffraction, XPS and solid-state NMR

A. Malki [a], Z. Mekhalif [b], S. Detriche [b], G. Fonder [b], A. Boumaza [a,*], A. Djelloul [a]

[a] Laboratoire des structures, propriétés et interactions inter atomiques (LASPI²A), Faculté des sciences et technologies, Université Abbes Laghrour, Khenchela 40000, Algérie

[b] Laboratoire de Chimie et Electrochimie des Surfaces, Facultés Universitaires Notre-Dame de la Paix, Rue de Bruxelles 61, B-5000 Namur, Belgium

ARTICLE INFO

Article history:
Received 17 November 2013
Received in revised form
1 March 2014
Accepted 7 March 2014
Available online 20 March 2014

Keywords:
Gibbsite
Transition alumina
X-ray diffraction
X-ray photoelectron microscopy
^{27}Al nuclear magnetic resonance

ABSTRACT

The changes caused by heat treatment of gibbsite powder at 300–1473 K were studied using the X-ray diffraction (XRD), X-ray photoemission (XPS) spectra and ^{27}Al magic angle spinning nuclear magnetic resonance spectroscopy (^{27}Al MAS NMR). XRD analysis indicates that the transformation sequence involves the formation of κ-Al_2O_3 as an intermediate phase between χ- and α-Al_2O_3. The crystallite size of χ-Al_2O_3 is as small as 10 nm. XPS analysis indicates that the ratio of aluminium atoms to oxygen atoms in χ-Al_2O_3 and κ-Al_2O_3 increases, whereas the expected ratio is observed in α-Al_2O_3. The percentage of AlO_4 units in the transition aluminas follows the same behaviour as the ratio of Al/O.

1. Introduction

Transition aluminas are typically used in industry as absorbents, catalysts, catalyst supports, coatings and soft abrasives due to their fine particle size, high surface area and catalytically active surfaces [1]. α-Al_2O_3 is used to manufacture ceramic materials with high thermal resistance for refractory, microelectronics and structural applications due to its stability and other beneficial characteristics. A growing number of these applications require a fundamental understanding of the properties of these compounds such as the crystal structure, particle size, surface area, reactivity, coordination spheres (AlO_4, AlO_5 and AlO_6), density, dielectric constant, energy gap, pore size and the degree of hydration of the surface. Gibbsite is the precursor of these aluminas. An important advantage of this hydroxide is that specific heat treatment can produce all of the transition aluminas via two routes [2–6]

gibbsite → χ-Al_2O_3 → κ-Al_2O_3 → α-Al_2O_3,

gibbsite → boehmite → γ-Al_2O_3 → δ-Al_2O_3 → θ-Al_2O_3 → α-Al_2O_3.

The formation of α-alumina by calcination of gibbsite comprises the intermediate steps. The different transition aluminas are formed and may even be present simultaneously. From a structural viewpoint, the transition aluminas are formed by arrangements of aluminium atoms in tetrahedral and octahedral sites surrounded by oxygen atoms. In α-Al_2O_3, all of the Al ions are octahedrally coordinated (AlO_6 units). However, tetrahedrally coordinated (AlO_4) units are found in transition aluminas. The number of occupied tetrahedral or octahedral sites varies for different polymorphs, which leads to remarkable differences in their properties such as the crystal packing, electronic structure and dielectric constant. χ-Al_2O_3 exists in the temperature range between 500 and 1143 K and at 543 K, the product still retains 13% of the water, which is gradually lost as the temperature increases to 1073 K. Between approximately 1243 and 1463 K, κ-Al_2O_3 is present [6]. The final product from the thermal decomposition of gibbsite is corundum, which has a hexagonal structure wherein all Al of the atoms are octahedrally coordinated [7].

Herein, we report the systematic characterisation of the different phases of alumina formed by calcination of gibbsite using XRD, XPS and ^{27}Al MAS-NMR. We carry out detailed analysis to determine an Al/O ratio and to estimate relative occupancy of tetrahedral and octahedral aluminium sites in aluminas.

2. Experimental techniques

2.1. Samples and treatments

Gibbsite powder ($Al_2(OH)_6$) with a density of ~2.4 g/cm³ from Biochem (C.A.S.: 21645-51-2, EINECS: 244-492-7) was used.

* Corresponding author.
E-mail address: charif_boumaza@yahoo.com (A. Boumaza).

http://dx.doi.org/10.1016/j.jssc.2014.03.019
0022-4596/

The powder is made of platelet aggregates having the chemical composition of 34.6% Al, 61.5% O, 3.9% H and max.: 0.002% (Fe), 0.004% (Cl), 0.04% SO_4, 0.005% heavy metals (as Pb) and 0.25% non precipitable by NH_4OH (as SO_4). The sample experienced an ignition loss of 32–35% at 1273 K and had a purity grade of 99.6%. Its average particle size (20 μm) was due to the agglomeration of crystallites. The specific surface area of the original sample was 0.5 m^2/g.

The experimental gibbsite micrometric powder was used to form metastable χ- and κ-aluminas and stable α-alumina via calcinations at various temperatures. The gibbsite powder was calcined in air at temperatures ranging from 373 to 1473 K according to the following heat treatment procedure:

- Heat to the specified temperature at 10 K/min.
- Maintained for 4 h at the calcination temperature.
- Rapidly cool to room temperature (air quench).
- The uncertainty in the temperature was $\Delta T = 2$ K.

2.2. Characterisation of samples

All of the samples were characterised using XRD, XPS spectroscopy and ^{27}Al MAS NMR spectroscopy.

X-ray diffraction analysis was performed with a PANalytical X'Pert ProMRD diffractometer with Cu*K*α radiation ($\lambda = 0.15418$ nm). The thermogravimetric (TG) data were recorded under a dry air flow with a heating rate of 10 K/min in a SETARAM TGDTA92 16.18 thermal analyser. TG measurements were corrected for temperature-dependent buoyancy by subtracting the data of a measurement carried out on an inert sample. An XPS K-Alpha spectrometer was used to qualitatively and quantitatively verify the composition of the different powder compounds. The spectra were treated using the Thermo Avantage V5.27 software. The photoelectrons are excited using a monochromatic Al *K*α radiation as the excitation source, collected at $\theta = 0^\circ$ with respect to the surface normal and detected with a hemispherical analyser. The spot size of the XPS source on the sample is 200 μm, and the analyser is operated with a pass energy of 150 eV for the survey spectra and 20 eV for the accumulation spectra of the core levels. The pressure is maintained below 1×10^{-8} Torr during data collection, and the binding energies (E_b) of the obtained peaks are referenced to the C1*s* signal for C–H, which is set to 285.0 eV. XPS measurements are made with uncertainties of about 0.1–0.2 eV. ^{27}Al MAS-NMR spectra were recorded with a Bruker Avance 500 spectrometer, and the experiments were conducted in a magnetic field of 11.7 T (^{27}Al Larmor frequency 130 MHz) and 3.2 probe spinning samples at 14 KHz. These spectra were referenced against $Al(NO_3)_3$ in solution at 0 ppm. A pulse width of 1 μs was used to yield a small tip angle of 10° with a recycle delay of 0.1 s and an overall acquisition time of 512 s for each sample.

3. Results and discussion

3.1. X-ray diffraction results

The gibbsite powder was calcined at various temperatures and characterised to determine the transition aluminas states that pass through prior to forming α-alumina. Diffraction analysis has played a central role in elucidating structural information in the transition aluminas as well as for determining the sequence of the structural changes and how these changes are influenced by various factors. For the treated gibbsite powder, X-ray analysis remains the main tool for examining the phase composition and determining the alpha alumina content. X-ray diffraction of the samples (Gibbsite (G), G373–G1373 and G1473; the number following G stands for the calcination temperature in Kelvin) are shown in Fig. 1a–d. Thermal evolution of the gibbsite powder structure in the range 300–1473 K by XRD patterns was investigated.

As shown in Fig. 1a (pattern (G)), all of the detectable peaks in this pattern can be assigned based on their peak position to gibbsite (γ-$Al_2(OH)_6$). The results in Fig. 1a are compared with the standard diffraction peaks from JCPDS Card no. 33-0018. The XRD patterns of gibbsite after heating at 473 K show a new peak at 14.49°(2θ) corresponding to bohemite (AlO(OH)) along with gibbsite peaks. Between 473 and 673 K, gibbsite converts to boehmite and amorphous aluminium oxide (may be χ-Al_2O_3), which is in agreement with the results from previous studies [5,8]. The XRD patterns of the 573 and 673 K samples are shown Fig. 1a and are in good agreement with the reference pattern (21-1307 JCPDS file) corresponding to the orthorhombic boehmite (AlO(OH)) structure. From approximately 773–1073 K, the patterns primarily corresponds to χ-Al_2O_3. The X-ray analysis demonstrates good agreement with the references of the files (04-0880 and 13-0373 JCPDS) corresponding to a cubic and hexagonal structure, respectively, for χ-Al_2O_3. At 773 K, the χ phase is expected (at 543 K; χ-Al_2O_3 approximate formula is $Al_2O_3 \cdot 0.75\ H_2O$ and at 1103 K, χ-Al_2O_3 formula is Al_2O_3) [6]. Gibbsite is the only aluminium hydroxide that produces χ-alumina crystals by thermal dehydroxylation (Fig. 1b). The proportion of tetrahedral sites is 29% χ-alumina [7]. Despite numerous studies, the crystal structure of χ-alumina is still uncertain. Stumpth et al. [9] assumed a cubic (not spinel) unit cell (04-0880 JCPDS file). However, two hexagonal structures have been suggested [6,10] (13-0373 JCPDS file). The XRD patterns of the 773, 873, 973, 1073 and 1173 K samples are shown in Fig. 1b and are in good agreement with the reference patterns (04-0880 JCPDS and 13-0373 JCPDS files) corresponding to the cubic and/or hexagonal χ-Al_2O_3 structures, respectively.

The quantity of γ-Al_2O_3 formed by conversion of boehmite was not sufficient for detection. The XRD patterns of gibbsite after heating at 1173 K show a new peak at 64.85°(2θ) corresponding to κ-Al_2O_3 along with χ-Al_2O_3 peaks. From Fig. 1c, κ-alumina is only formed from heating the χ-alumina phase, and the crystal structure of κ–alumina is well known [11–14]. For gibbsite heated in air at 1273 and 1373 K, the κ phase is expected (Fig. 1d). The XRD pattern of the 1273 K sample is shown Fig. 1c and is in good agreement with the reference pattern (01-088-0107 JCPDS file). δ-Al_2O_3 and θ-Al_2O_3 are not observed at this temperature. When gibbsite is heated at 1373 K for 4 h, the peaks corresponding to α-Al_2O_3 appeared along with κ-Al_2O_3 peaks, and at 1473 K, only alpha alumina is present. The XRD pattern of α-Al_2O_3 (Fig. 1d (pattern (G1473)) is consistent with the reference XRD pattern for α-Al_2O_3 (46-1212 JCPDS file). Alpha alumina, or corundum, is the most stable phase of alumina.

Information on the crystallite size (D) for the compounds (i.e., gibbsite, boehmite, χ-Al_2O_3, κ-Al_2O_3 and α-Al_2O_3) was obtained from the full-width at half-maximum of the diffraction peaks using the Scherrer formula [15]:

$$D = \frac{0.94\lambda}{\beta_{(hkl)} \cos \theta_{(hkl)}}$$

where λ, $\theta_{(hkl)}$ and $\beta_{(hkl)}$ are the X-ray wavelength (0.15418 nm), Bragg diffraction angle and line width at half maximum, respectively. The values of the $\beta_{(hkl)}$ and $\theta_{(hkl)}$ parameters from the XRD peak are estimated by Gaussian fitting. This formula is not limited by the preferential orientation and is valid for an ordinary XRD profile. To improve the statistics, the most intense peaks in the profiles were chosen to determine the crystallite size. The gibbsite 002, 110 and 200 peaks, the boehmite 020, 120 and 031 peaks, the χ-alumina 200, 104, 214 peaks, the κ-alumina 022, 122 and 132 peaks, and the alpha alumina 012, 104, 113, 024 and 116 peaks

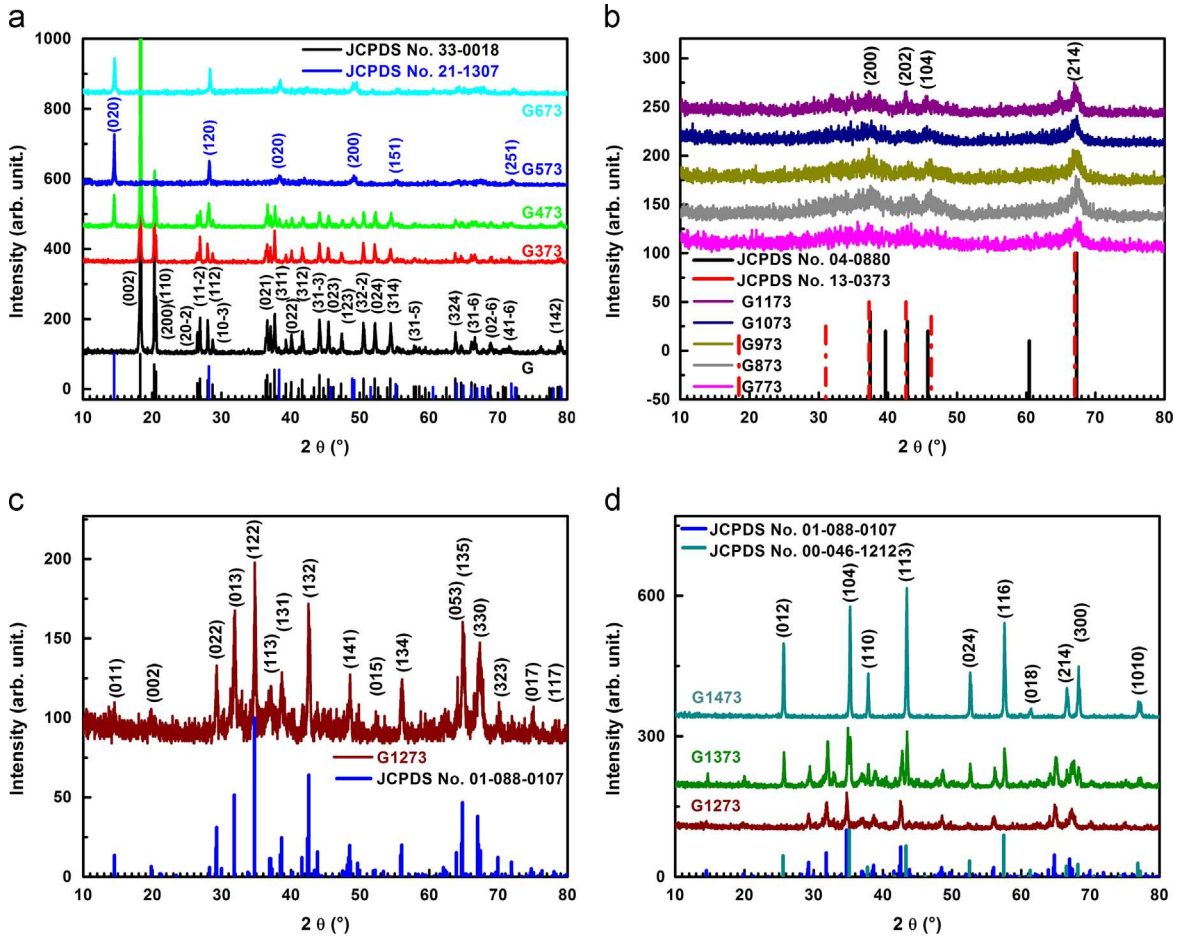

Fig. 1. XRD powder patterns of gibbsite untreated and heat-treated in air from 373 to 1473 K.

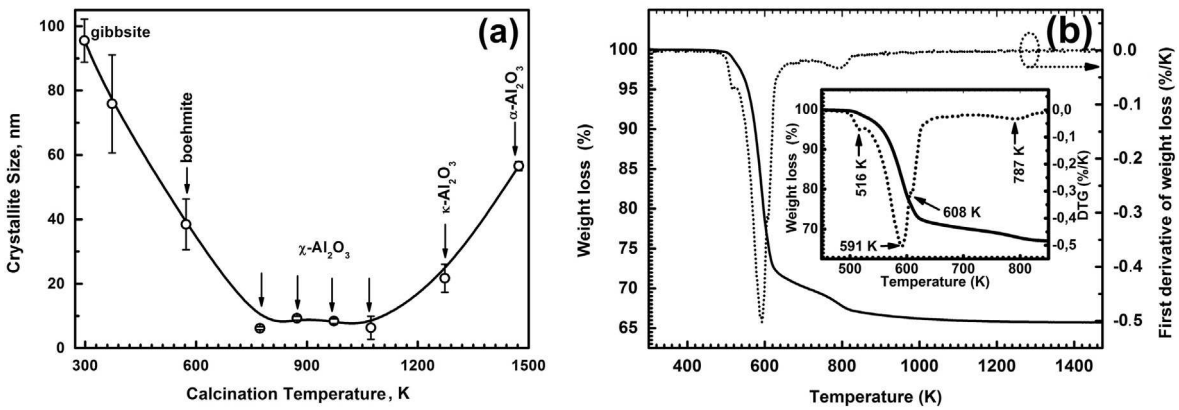

Fig. 2. Crystallite size of the compounds as a function of calcination temperature (a) and thermogravimetric (TG) curve for gibbsite at 10 K/min (b). Error bars in Fig. 2a indicate the standard deviation (SD).

were used in the determination of crystallite sizes for these materials.

The calculated crystallite size of the compounds as a function of calcination temperature is shown in Fig. 2a. It is worthy noted that the crystallite size decreases, from 95.5 ± 6.7 to 6.3 ± 3.6 nm, up to a calcination temperature of 1073 K and then increases to reach 56.5 ± 1.4 nm at 1473 K.

It has been reported that α-Al_2O_3 can be obtained directly from χ-Al_2O_3 bypassing the κ-Al_2O_3 intermediate phase when its crystallite size is as small as 10 nm [16,17]. XRD analysis indicates that the transformation sequence involves the formation of κ-Al_2O_3 as an intermediate phase between χ- and α-Al_2O_3 even though the crystallite size of χ-Al_2O_3 is less than or equal to 8 nm.

3.2. Thermogravimetric analysis

Fig. 2b show the typical thermogravimetric (TG) curve and first derivative of the weight loss (DTG) plot for gibbsite. TG curve and DTG plot are indicated as solid and dotted lines, respectively. The TG–DTG can be interpreted as follows: the gibbsite decomposition takes place in several steps. At a temperature slightly above 470 K, boehmite appears. In the range of 473–555 K, only a small weight

loss is observed (about 5%). This is due to the fact that not all the water is released. As the temperature increases above 555 K, the coarse gibbsite particles shatter, releasing water vapour. This is manifested by the fast weight loss on the TG curve of gibbsite (≈ 18% between 555 and 628 K). Up to the end temperature of the third DTG peak (608 K), the cumulative weight loss of the sample was 23.9%, which approached the theoretical weight loss from the conversion of $Al(OH)_3$ to AlO(OH) (23.09%). The formation of boehmite occurs when calcining between 473 and 673 K (see Fig. 1a). The DTG peak with maxima at ≈ 787 K (about 32% weight loss) of sample is due to χ-Al_2O_3 formation. This structure was confirmed by X-ray diffraction. The last step (830–1473 K) appears as a continuous weight loss (about 2%) which corresponds to the elimination of residual hydroxyls. The XRD patterns of gibbsite after heating at 1273 K shows the formation of κ-Al_2O_3 and after heating at 1373 K shows the new peaks corresponding to α-Al_2O_3 along with κ-Al_2O_3 peaks. Finally, the formation of α-Al_2O_3 occurs at 1473 K. The expected theoretical loss due to dehydration of gibbsite is 34.6%; the experimental loss is 34.3% a little lower. This difference of 0.3% is a bit larger than the experimental uncertainty 0.1%, the starting gibbsite may be slightly dehydrated.

3.3. X-ray photoelectron spectroscopy analysis

The XPS analysis of aluminium oxides and hydroxides was performed and interpreted for the O1*s*, C1*s* and Al2*p* bands. X-ray photoelectron spectra of hydrated alumina (gibbsite), heat-treated gibbsite (transition aluminas; χ and κ-Al_2O_3) and corundum (α-Al_2O_3) have been studied by spectral characterisation of each compound. Fig. 3a shows the XPS survey spectra of the untreated and calcined gibbsite. For gibbsite, the spectrum reveals photoemission peaks for O1*s*, C1*s*, S2*s*, S2*p*, Al2*s* and Al2*p*, which indicates the presence of O, C, S and Al on the surface of the untreated and heat treated gibbsite compounds. At 871 K, the aluminium to oxygen atom ratio was higher than that of stoichiometric Al_2O_3 (Fig. 3b). The aluminium to oxygen atom ratio increased as the calcination temperature increased. Between 300 and 1473 K prior to reaching the final ratio of the alpha alumina, the Al/O passes through two different levels. In the first step between 300 and 773 K, mixtures of hydroxides and amorphous oxides are present. The second step between 773 and 1373 K corresponds to the formation of transition aluminas (Chi, Kappa alumina and mixtures of oxides) (see Fig. 1b–d). The surfaces of compounds do not follow the stoichiometry of the bulk. The nonstoichiometry ($Al/O > 2/3$) can be explained by the formation of the clusters on aluminas surface. They can be represented by the formula $(Al_2O_3)_n(AlO)_x$ with $n=1$–7 and $x=1, 2, 3$. Fig. 3c shows the variation of the Al/O atomic ratios of these clusters compared with those obtained experimentally (XPS results) versus the cluster size (n). The Al/O atomic ratios of $(Al_2O_3)_n(AlO)_x$ clusters are in good agreement with those determined from XPS analyses. Chemical analysis of gibbsite indicates a deviation from stoichiometry with an Al/O atomic ratio of 0.368 compared to 0.333 in the stoichiometric case. A deficit of aluminium with an Al/O ratio of 0.655 (0.666 for the stoichiometric case) is observed during the formation of alpha alumina at 1473 K. The surface charging leads to the creation of oxygen vacancies and a loss of oxygen in the surface region when the surface is highly charged.

The XPS Al2*p* and Al2*s* spectra for untreated and heat-treated gibbsite at various temperatures (from 373 to 1473 K) for 4 h are

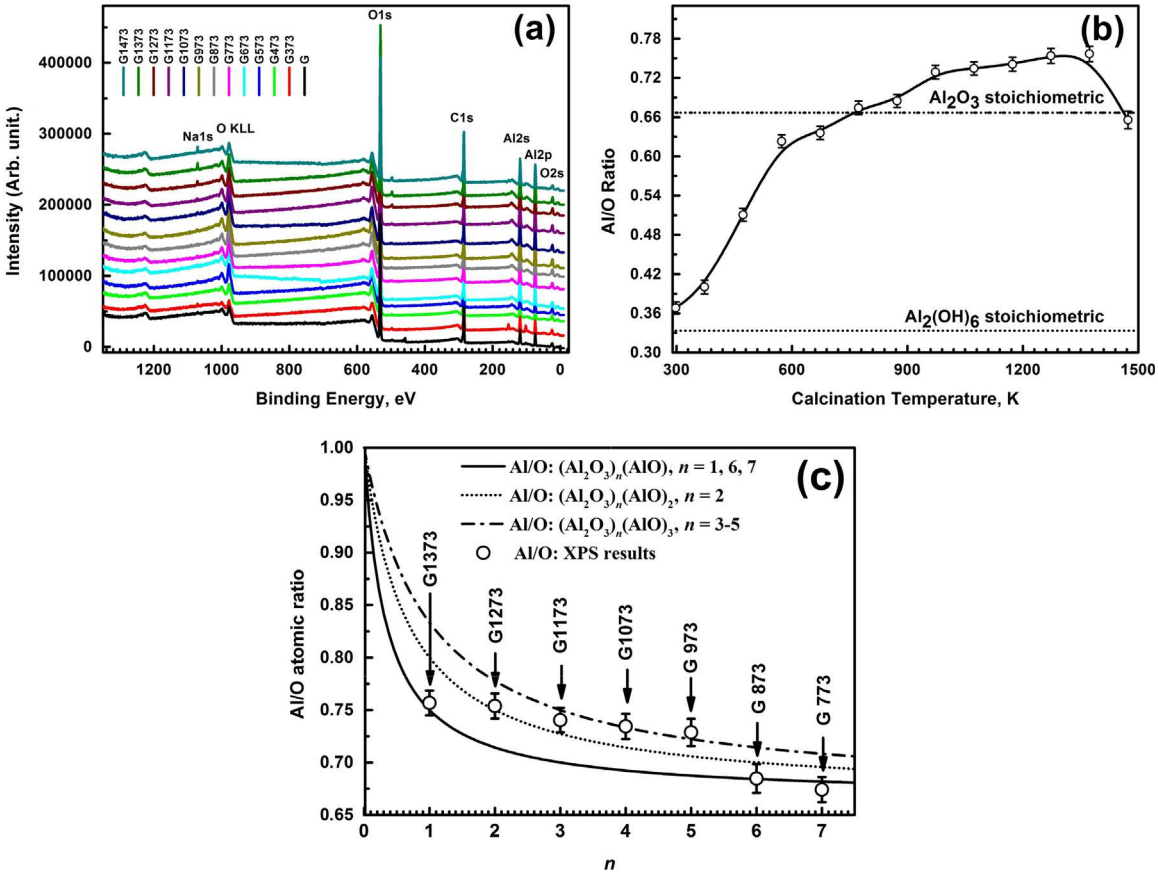

Fig. 3. XPS survey spectra of untreated and calcined gibbsite (a), aluminium to oxygen atom ratio in calcined gibbsite powder as a function of calcination temperature (b) and variation of the Al/O atomic ratios of $(Al_2O_3)_n(AlO)_x$ clusters compared with those obtained experimentally (XPS results) versus the cluster size (n) (c). Error bars in Fig. 3b indicate the standard deviation.

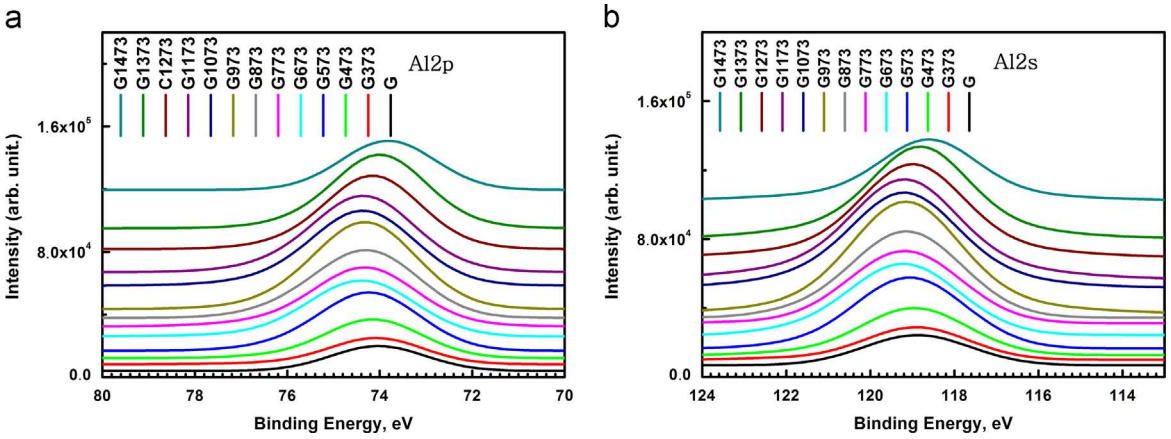

Fig. 4. XPS spectra in the Al2*p* (a) and Al2*s* (b) region for untreated and treated gibbsite at various temperatures.

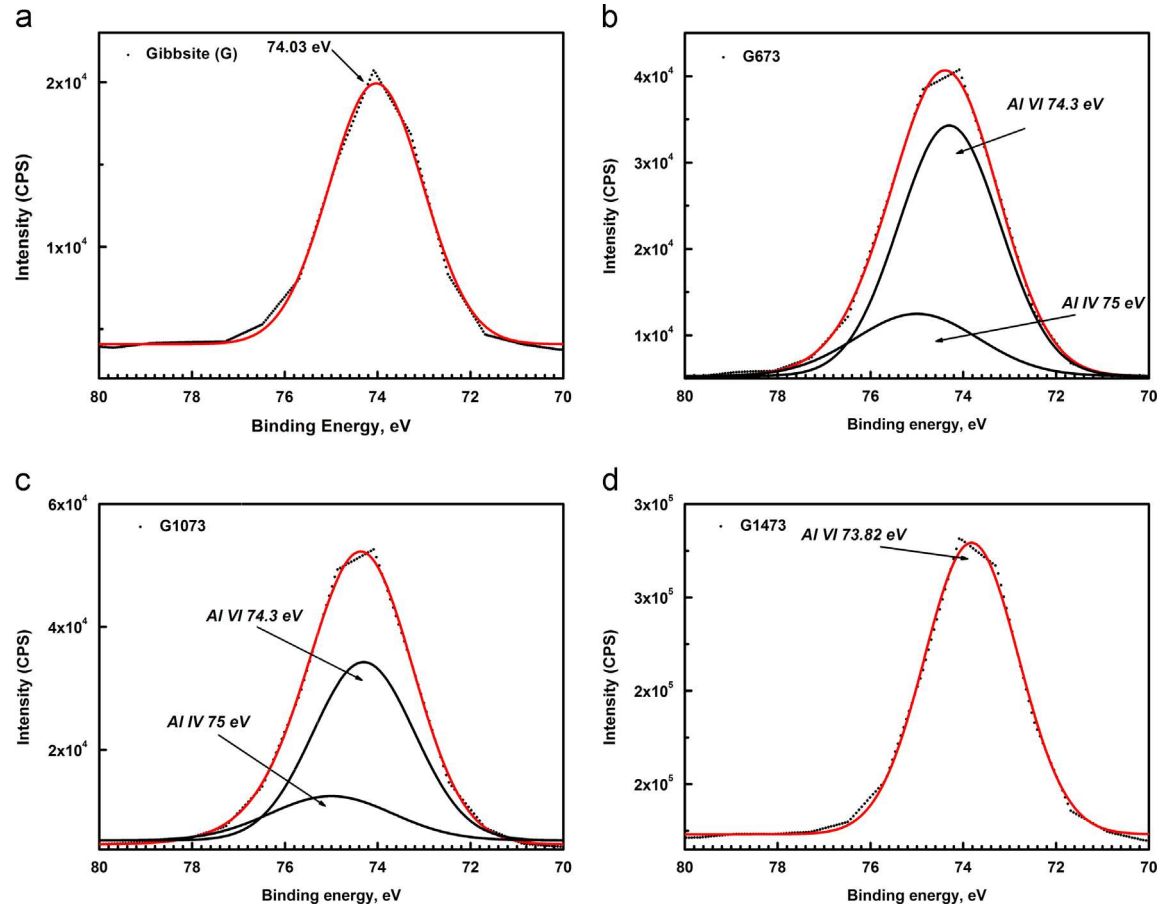

Fig. 5. Decomposed Al2*p* peaks of heat treated gibbsite (a) untreated, (b) calcined at 673 K, (c) calcined at 1073 K and (d) calcined at 1473 K. Experimental data points (full circles), decomposition components (black lines) and the fit to the data (red line) are shown. (For interpretation of the references to colour in this figure legend, the reader is referred to the web version of this article.)

shown in Fig. 4. Fig. 5 shows the decomposed Al2*p* peaks of the untreated and heat-treated gibbsite. The Al2*p* spectra are shifted 0.2 eV to a higher binding energy (E_b) in the order of α-Al_2O_3 < transition aluminas < gibbsite. A single band is observed for the starting gibbsite (Fig. 5a), and the peak is located at 74.03 eV (full width at half maximum (FWHM) 2.38 eV).

The aluminium in the transition aluminas can be present in two different positions. First, hexacoordinate aluminium can be present in the octahedral sheet, and second, tetracoordinate aluminium can be present in the tetrahedral sheet. As shown in Fig. 5b and c, the peaks for these valences are localised at 74.3 eV (FWHM 2.52 eV) and 75 eV (FWHM 3.47 eV) corresponding to the Al IV and Al VI states, respectively. A single band was observed for alpha alumina (Fig. 5d), which is obtained at a binding energy of 73.82 eV (FWHM 2.39 eV). The shapes of the Al2*p* and Al2*s* bands result in similar changes in gibbsite during calcination treatments. For these compounds, the results obtained for the valence Al2*p* indicate that the variations in binding energies are within an interval of approximately 1 eV, which are in good agreement with previous observations [18–20].

A detailed XPS study of treated gibbsite was performed. The XPS O1*s* and O2*s* spectra are shown in Fig. 6a and b. The O1*s*

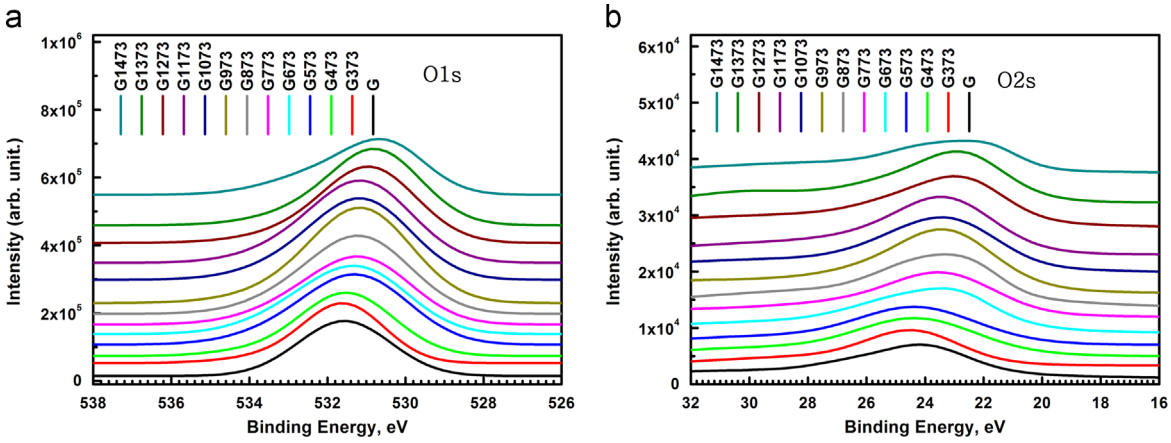

Fig. 6. XPS spectra in the O1*s* (a) and in the O2*s* (b) region for untreated and heat treated gibbsite at various temperatures.

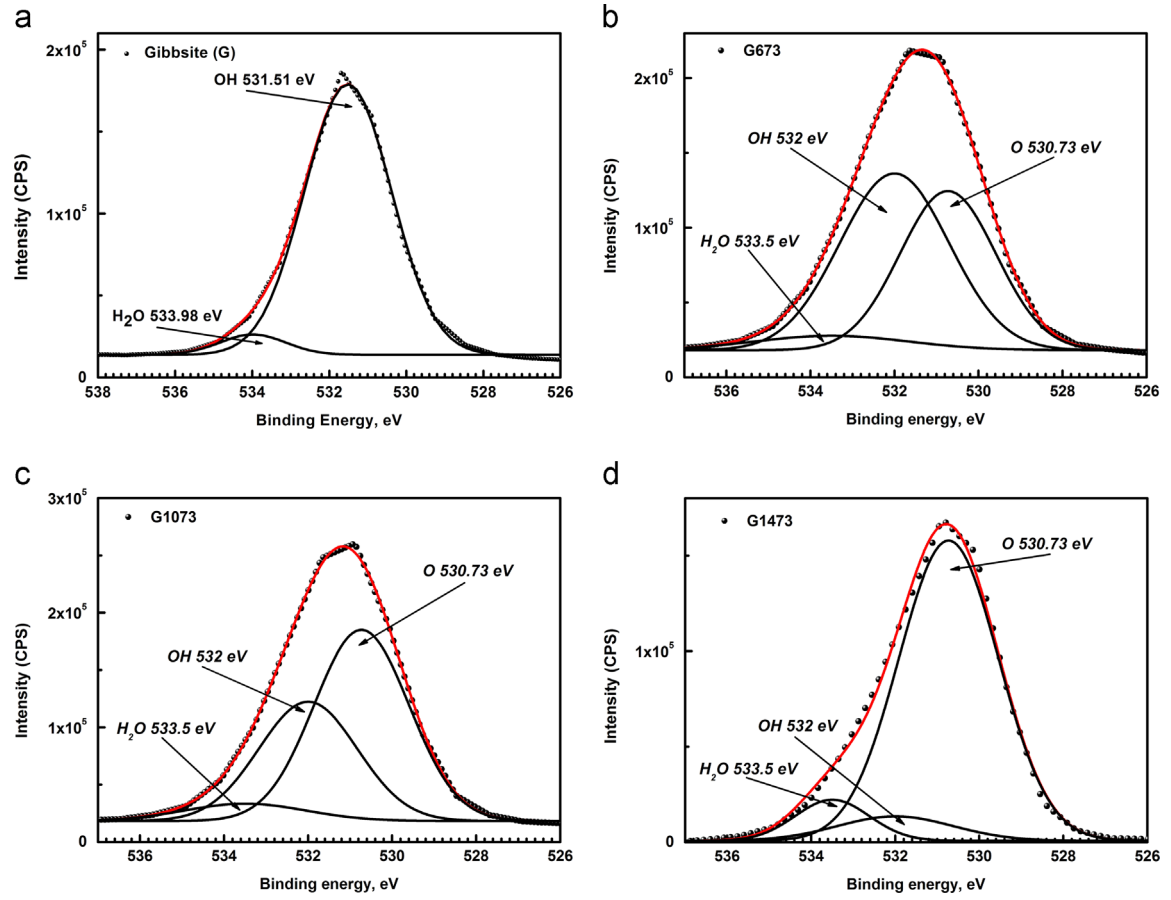

Fig. 7. Decomposed O1*s* peaks of heat treated gibbsite (a) untreated, (b) calcined at 673 K, (c) calcined at 1073 K and (d) calcined at 1473 K. Experimental data points (full circles), decomposition components (black lines) and the fit to the data (red line) are shown. (For interpretation of the references to colour in this figure legend, the reader is referred to the web version of this article.)

spectra are shifted 1 eV to a higher binding energy (E_b) in the order of α-Al_2O_3 < transition aluminas < gibbsite. The O1*s* peaks are less symmetrical (relative to peak Al2*p*), more complex and more sensitive to the different states of the minerals. In fact, the O1*s* band is very important due to its intensity, which allows it to be more sensitive and hence more exploitable. According to the literature, this band can be decomposed into two or three parts. The O1*s* band corresponding to oxides is located at ~531eV, the O1*s* band corresponding to the OH groups is located at ~532 eV, and the O1*s* band indicating the presence of amorphous mixtures containing H_2O is located at 533.5 eV [18].

Fig. 7 represents the decomposed O1*s* peaks of untreated and heat-treated gibbsite. We note that these peaks exhibit significant differences depending on the compound. In crystallised gibbsite platelets, the energy of O1*s* is shifted to 531.51 eV corresponding to the OH group in the crystal structure of aluminium hydroxide. A mixture of adsorbed water, amorphous precipitates and oxygen impurities was observed at 533.98 eV (Fig. 7a). These values are in agreement with the literature data [18–22]. The transition aluminas bands are broad and intense indicating the presence of three compounds (i.e., oxides, hydroxides and H_2O), and decomposition of these peaks yields the corresponding positions with binding

energies of 530.7 eV (FWHM 2.66 eV), 532 eV (FWHM 2.76 eV) and 533.5 eV (FWHM 3.39 eV), respectively (Fig. 7b–d).

The Cls core level photoemission spectra for gibbsite and calcined gibbsite are shown in Fig. 8a. Peak fitting is required to analyse the carbon components. In the literature, six component peaks at binding energies of 290–284.0 eV correspond to the C–C, C–H, C–OR, C–OH, C═O and COOR bonds, respectively. These surface carbons are common contaminations from hydrocarbons and carboxylic acid when CO_2 reacts with air and moisture. The decomposition of the C1*s* signal in the domain (calcined gibbsite at 1473 K) results in three bands (Fig. 8b). The peak at 285.0 eV is associated with the binding energy of the C atoms in aromatic C–C/C–H, the peak at 286.19 eV can be attributed to the binding energy of the C–O group, and the peak at 288.55 eV can be attributed to the binding energy of the carboxylic group (O–C═O), which is in agreement with the literature results [23–25].

3.4. *^{27}Al magic angle spinning nuclear magnetic resonance spectroscopy (^{27}Al MAS NMR) analysis*

Information on the relative occupancy of tetrahedral and octahedral aluminium sites in aluminas was obtained using ^{27}Al solid-state MAS NMR. The chemical shift ranges for aluminium in different coordinations with oxygen (or hydroxyls) are typically −10 to 20 ppm for octahedrally coordinated aluminium (AlO_6), 30–40 ppm for pentahedral coordinated aluminium (AlO_5) and 50–80 ppm for tetrahedrally coordinated aluminium (AlO_4) [26]. Fig. 9 shows the ^{27}Al MAS NMR spectra of untreated and heat-treated gibbsite. The peaks related to the AlO_6 units are rather thin for the G, G373 and G473 samples but widen progressively as the temperature increases with the largest peak located at 1027 K. At 1473 K, the peak of alpha alumina is the only symmetric one. The spectra for the as-received gibbsite (untreated) and G373 are shown in Fig. 9a. The central peak is asymmetric with an observed peak shift of 8.63 ppm and a small shoulder at 2.2 ppm. This peak position is consistent with hexacoordinate (octahedral, AlO_6) aluminium cations, which is consistent with the results from diffraction studies. The peaks (G473 spectrum) for the hexacoordinate Al in the mineral overlap in the mixture (gibbsite+boehmite). This peak position is only consistent with hexacoordinate (AlO_6) aluminium cations. The peaks (G573 and G673 spectra) for hexacoordinate A1 in the treated gibbsite overlap in the mixture (Boehmite+chi). The peak assigned to the tetracoordinate Al appears when chi-alumina is present. The spectra of the G773, G873, G973 and G1073 samples (containing chi- and small amount of kappa alumina) have peaks located at 8.62 and 65.53 ppm, which correspond to hexacoordinate and tetracoordinate Al, respectively. The spectrum of the G1173 sample (containing chi- and kappa aluminas) exhibits peaks located at 8.86 and 65.91 ppm, which correspond to hexacoordinate and tetracoordinate Al, respectively. The spectrum of the G1273 sample (containing kappa-alumina) contains peaks located at 8.48 and 66.17 ppm,

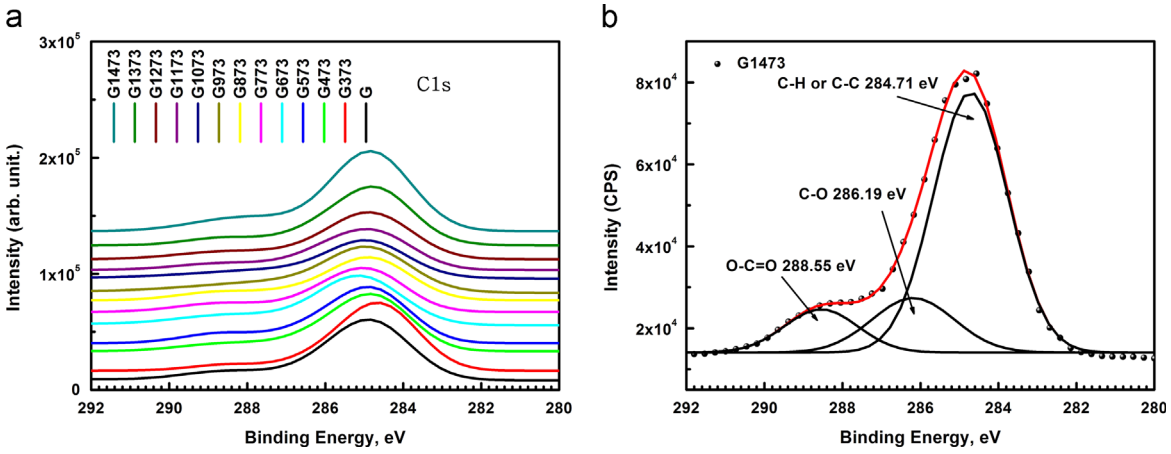

Fig. 8. XPS spectra in the C1*s* in the region for untreated and treated gibbsite at various temperatures (a) and decomposition of the C1*s* peak (b). Experimental data points (full circles), decomposition components (black lines) and the fit to the data (red line) are shown. (For interpretation of the references to colour in this figure legend, the reader is referred to the web version of this article.)

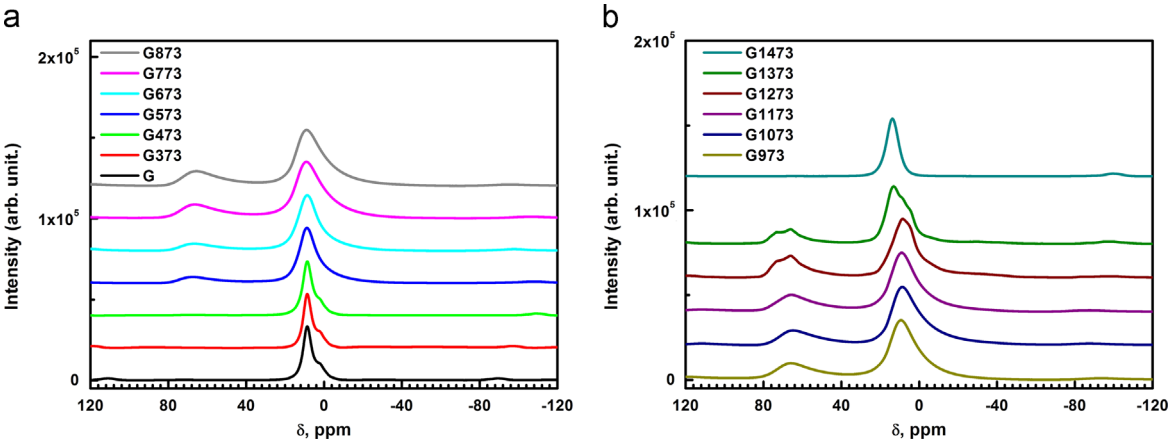

Fig. 9. ^{27}Al MAS NMR spectra of untreated and heat treated gibbsite in air from 373 to 1473 K.

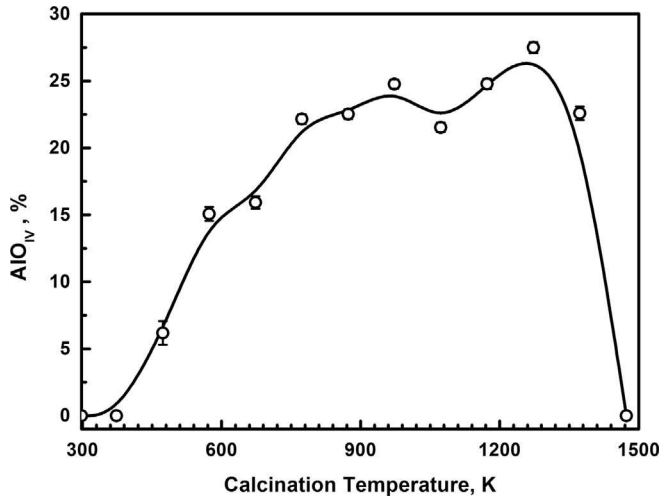

Fig. 10. The percentage of AlO_4 content in the ^{27}Al MAS NMR spectra as a function of calcination temperature. Error bars indicate the standard deviation.

which correspond to hexacoordinate and tetracoordinate Al, respectively, and a small shoulder at 4.53 ppm, which corresponds to hexacoordinate Al. The spectrum for the G1373 sample (containing kappa, small amount of alpha alumina) exhibits peaks located at 12.92 and 66.19 ppm, which correspond to hexacoordinate and tetracoordinate Al, respectively, and two small shoulders at 8.36 and 4.85 ppm, which corresponds to hexacoordinate Al. The eventual formation of crystalline α-$A1_2O_3$ (corundum) is clearly shown in the MAS NMR spectrum (Fig. 9b) by the narrower and more symmetric resonances indicating longer-range structure and a characteristic peak position at 13.7 ppm.

By integrating the peak areas, the ^{27}Al tetrahedral/octahedral ratio has been determined. The percentage of AlO_4 content as a function of calcination temperature is shown in Fig. 10, and it does not vary significantly between 750 and 1200 K. The proportion of tetrahedral sites is ~22% and ~27% in χ- and in κ-$A1_2O_3$, respectively.

The percentage of AlO_4 units in the transition aluminas follows the same behaviour as the ratio of Al/O.

4. Conclusion

Gibbsite was calcined at 300–1473 K, and the relationships between the calcination temperature and various properties of this compounds have been examined by various techniques to elucidate their roles in the expected gibbsite transformations leading to transition aluminas and ultimately to alpha alumina. XRD analysis indicates that the transformation sequence involves the formation of κ-Al_2O_3 as an intermediate phase between χ- and α-Al_2O_3. The crystallite size of χ-Al_2O_3 is as small as 10 nm. The determination by XPS of an Al/O ratio higher than 2/3 in the samples annealed between 800 K and 1400 K, whereas the expected ratio is observed after the full conversion to α-Al_2O_3. The nonstoichiometry (Al/O > 2/3) can be explained by the formation of the clusters on aluminas surface. They can be represented by the formula $(Al_2O_3)_n(AlO)_x$ with $n=1$–7 and $x=1, 2, 3$. Information on the relative occupancy of tetrahedral and octahedral aluminium sites in aluminas was obtained using ^{27}Al solid-state MAS NMR. The percentage of AlO_4 units in transition aluminas follows the same behaviour as the ratio of Al/O.

References

[1] R.S. Zhou, R.L. Snyder, Acta Cryst. B 47 (1991) 617–630.
[2] K. Wefers, C. Misra, Alcoa Technical Paper 19, Revised, Aluminium Company of America, Pennsylvania, 1987, pp. 54–58.
[3] B. Whittington, D. Ilievski, Chem. Eng. J. 98 (2004) 89–97.
[4] V.J. Ingram-Jones, R.C.T Slade, T.W. Davies, J.C. Southern, S. Salvador, J. Mater. Chem. 6 (1996) 73–79.
[5] A.C. Vieira Coelho, H.D. Souza Santos, P.K. Kiyohara, K.N.P. Marcos, P.D. Souza Santos, Mater. Res. 10 (2) (2007) 183–189.
[6] G.W. Brindley, J.O. Choe, Am. Mineral. 46 (1961) 771–785.
[7] H. Wang, B. Xu, P. Smith, M. Davies, L. DeSilva, C. Wingate, J. Phys. Chem. Solids 67 (2006) 2567–2582.
[8] B.C. Lippens, J.H. De Boer, Acta Cryst. 17 (1964) 1312–1321.
[9] H.C. Stumpf, A.S. Russell, J.W. Newsome, C.M. Tucker, Ind. Eng. Chem. 42 (1950) 1398–1403.
[10] H. Saalfeld, Neues Jahrb. Mineral. Abh. 95 (1960) 1–87.
[11] R. Vali, S.M. Hosseini, Comp. Mater. Sci. 29 (2004) 138–144.
[12] L. Favaro, A. Boumaza, P. Roy, J. Lédion, G. Sattonnay, J.B. Brubach, A.M. Huntz, R. Tetot, J. Solid State Chem. 183 (2010) 901–908.
[13] Y. Yourdshahyan, U. Engberg, L. Bengtsson, B.I. Lundqvist, B. Hammer, Phys. Rev. B 55 (14) (1997) 8721–8725.
[14] P.S. Santos, H.S. Santos, S.P. Toledo, Mater. Res. 3 (2000) 104–114.
[15] B.D. Cullity, Elements of X-Ray Diffraction, 2nd ed., Addison-Wesley, Reading, MA (1978) 102.
[16] M. Inoue, H. Kominami, T. Inui, J. Am. Ceram. Soc. 75 (9) (1992) 2597–2598.
[17] P.L. Chang, Y.C. Wu, S.J. Lai, F.S. Yen, J. Eur. Ceram. Soc. 29 (16) (2009) 3341–3348.
[18] J.T. Kloprogge, L.V. Duong, B.J. Wood, R.L. Frost, J. Colloid Interface Sci. 296 (2006) 572–576.
[19] A. Strålin, T. Hjertberg, Appl. Surf. Sci. 74 (1994) 263–275.
[20] B.R. Strohmeier, Surf. Interface Anal. 15 (1990) 51–56.
[21] D. Yang, M. Krasowska, R. Sedev, J. Ralston, Phys. Chem. Chem. Phys. 12 (2010) 13724–13729.
[22] J. Hu, X.H. Zhao, S.W. Tang, W.C. Ren, Z.Y. Zhang, Appl. Surf. Sci. 253 (2007) 8879–8884.
[23] S. Ben Amor, G. Baud, M. Jacquet, G. Nanse, P. Fioux, M. Nardin, Appl. Surf. Sci. 153 (2000) 172–183.
[24] C. Ma, Y. Chang, W. Ye, W. Shang, C. Wang, J. Colloid Interface Sci. 317 (2008) 148–154.
[25] F. Monteil-Rivera, E.B. Brouwer, S. Masset, Y. Deslandes, J. Dumonceau, Anal. Chim. Acta 424 (2000) 243–255.
[26] S. Acosta, R.J.P. Corriu, D. Leclercq, P. Lefèvre, P.H. Mutin, A. Vioux, J. Non-Cryst. Solids 170 (1994) 234–242.